ChemComm

Switching the selectivity of the photoreduction reaction of carbon dioxide by controlling the band structure of a g-C$_3$N$_4$ photocatalyst†

Ping Niu,[a] Yongqiang Yang,[a] Jimmy C. Yu,[b] Gang Liu*[a] and Hui-Ming Cheng[ac]

The selectivity of the CO$_2$ photoreduction reaction in the presence of water vapour can be modulated by the band structure of a g-C$_3$N$_4$ photocatalyst. The major products obtained using bulk g-C$_3$N$_4$ with a bandgap of 2.77 eV and g-C$_3$N$_4$ nanosheets with a bandgap of 2.97 eV are acetaldehyde (CH$_3$CHO) and methane (CH$_4$), respectively.

Photocatalytic reduction of CO$_2$ to fuels using sunlight is an ideal solution to the global warming and energy problems. In this approach, the reduction of CO$_2$ can take place on the solid–liquid interface or the solid–gas interface of semiconductor photocatalysts.[1–3] It is a complex reaction involving multiple-electron transfers, leading to a mixture of products such as carbon monoxide, organic compounds including formic acid (HCOOH), formaldehyde (HCHO), methanol (CH$_3$OH), methane (CH$_4$) as well as higher hydrocarbons. These organic compounds are fuels with different energy densities, and they are also important industrial chemicals. Concerning the practical use of these compounds, it is essential to produce them to be as pure as possible. This requires the development of photocatalysts with high selectivity for a specific product. Unfortunately, little is known about the crucial factors controlling the selectivity of the photocatalytic CO$_2$ reduction. Revealing these crucial factors is therefore important but it remains a great challenge.

For a single-component photocatalyst, there are many factors that can affect its reaction selectivity. A previous study shows that modifying the surface atomic structure of anatase TiO$_2$ microspheres with dominant {001} facets by introducing fluorine can sensitively change the adsorption capability towards azo dyes and thus realize the selective decomposition of different dyes.[4]

An example of the effect of changing the surface band structure in modulating the preference of photocatalytic reduction and oxidation is that the downward shift of the band edges of the surface layer of anatase TiO$_2$ microspheres by introducing boron can lead to switching of the preference towards photocatalytic hydrogen and oxygen producing reactions from splitting water.[5] These results strongly suggest that surface atomic structure and band structure are the two important factors to be considered in designing photocatalysts for specific reactions because they intrinsically determine the adsorption of the reactant molecules and the redox potentials of charge carriers in photocatalysts.

Photoreduction of CO$_2$ is usually conducted on transition metal oxides and their derivatives (*i.e.*, doped ones), though some sulfides and phosphides have been explored as photocatalysts for CO$_2$ reduction.[2,3] Graphitic-C$_3$N$_4$ (g-C$_3$N$_4$) with a bandgap of *ca.* 2.7 eV[6] has emerged as an attractive visible light photocatalyst for photocatalytic hydrogen evolution,[6–10] decomposition of pollutants,[11–13] organic synthesis[14] and optoelectronic conversion[15] because its high conduction band minimum favors the reduction half-reaction. It is also used for CO$_2$ photoreduction or CO$_2$ conversion.[16–21] Moreover, a layered structure makes it easy to tailor its band structure by controlling its thickness without changing the atomic structure. All these properties make g-C$_3$N$_4$ a good platform to study the effect of band structure on the selectivity of CO$_2$ photoreduction.

In this work, two g-C$_3$N$_4$ photocatalysts with different band structures, namely, bulk g-C$_3$N$_4$ and g-C$_3$N$_4$ nanosheets with bandgaps of 2.77 eV and of 2.97 eV (Fig. 1) were used to study the effect of the band structure of photocatalysts on the selectivity of the photoreduction of CO$_2$. Bulk g-C$_3$N$_4$ was synthesized through the thermal condensation of dicyandiamide in air according to a reported procedure.[6] The synthesis of the nanosheets was conducted using a simple top-down strategy developed in our previous study,[22] namely the thermal oxidation etching of bulk g-C$_3$N$_4$ in air. The resultant nanosheets have a very similar geometric structure to their parent bulk g-C$_3$N$_4$. One distinctive feature of the nanosheets obtained from the bulk is a 0.2 eV larger bandgap associated with their small thickness of around 2 nm.

^{a} *Shenyang National Laboratory for Materials Science, Institute of Metal Research, Chinese Academy of Sciences, 72 Wenhua RD, Shenyang 110016, P. R. China. E-mail: gangliu@imr.ac.cn; Fax: +86 24 23971682; Tel: +86 24 23971088*

^{b} *Department of Chemistry and Institute of Environment, Energy and Sustainability, The Chinese University of Hong Kong, Shatin, New Territories, Hong Kong, China*

^{c} *Chemistry Department, Faculty of Science, King Abdulaziz University, Jeddah 21589, Saudi Arabia*

† Electronic supplementary information (ESI) available: Experimental details, SEM images, XRD patterns and XPS spectra. See DOI: 10.1039/c4cc03060e
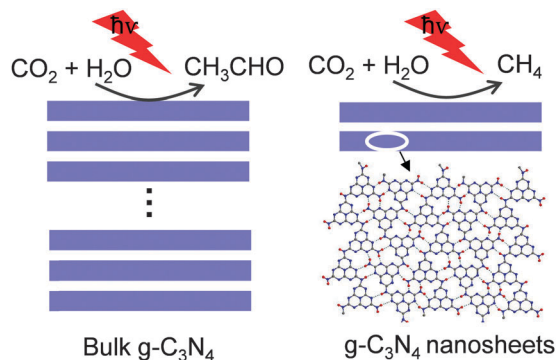
Fig. 1 Schematic of the generation of CH_4 and CH_3CHO on bulk g-C_3N_4 and a g-C_3N_4 nanosheets in the photoreduction of CO_2 in the presence of water vapor.
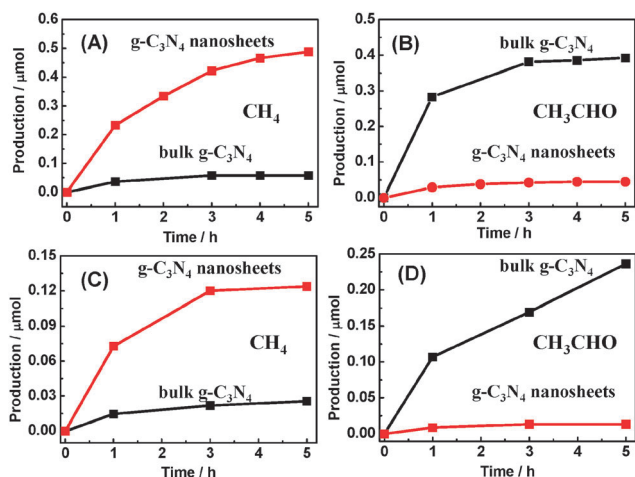
Fig. 2 Irradiation time-dependent generation of CH_4 and CH_3CHO for bulk g-C_3N_4 and g-C_3N_4 nanosheets in the photoreduction of CO_2 under (A, B) UV-visible light and (C, D) visible light ($\lambda > 400$ nm).

The characteristics of the photoreduction reaction of CO_2 were studied in a solid–gas reaction system containing the g-C_3N_4 photocatalyst, CO_2, and water vapor. Fig. 2 shows the irradiation time-dependent generation of products using the two g-C_3N_4 photocatalysts. In all cases, CH_4 and CH_3CHO are the two major carbon–hydrogen containing products. Under UV-visible light, the nanosheets show a high selectivity toward the generation of CH_4 (Fig. 2A) while the bulk g-C_3N_4 has a preference toward the production of CH_3CHO (Fig. 2B). The generation rate of CH_4 with the nanosheets is more than an order of magnitude higher than that of the bulk g-C_3N_4. In contrast, the generation rate of CH_3CHO with the nanosheets is an order of magnitude lower than that of bulk g-C_3N_4. Similar trends were also observed under visible light (Fig. 2C and D), although the absolute generation rates of CH_4 and CH_3CHO for the nanosheets and bulk g-C_3N_4 are much lower than those under UV-visible light. These results clearly suggest that g-C_3N_4 photocatalysts with different band structures have different effects on CO_2 photoreduction, which is independent of the wavelength of light irradiation. Control experiments showed no activity in generating CH_4 and CH_3CHO in the absence of g-C_3N_4 or CO_2 or light irradiation. All these results indicate that g-C_3N_4 is

photocatalytically active in reducing CO_2 and its selectivity of the photoreduction reactions is associated with its bandgap. On the other hand, the competitive hydrogen production during the CO_2 photoreduction was estimated as shown in Fig. S1 (ESI†). Under UV-visible light the nanosheets give a hydrogen production rate comparable to that of their CH_4 production. The nanosheets show much higher hydrogen production rates than bulk g-C_3N_4 under both UV-visible light and visible light. This is largely because of the advantageous band structure of the nanosheets and also the large surface area.

Prior to an analysis of the origin of the reaction selectivity, it is necessary to investigate the stability of g-C_3N_4 photocatalysts in the photoreduction of CO_2 in terms of their morphology, crystal structure and chemical state. Fig. S2 (ESI†) shows scanning electron microscopy images of two g-C_3N_4 photocatalysts before and after the reactions. Compared to the fluffy state of the nanosheets, bulk g-C_3N_4 appears as particles of several micrometers width. No detectable change was observed after the reactions. X-ray diffraction (XRD) patterns (Fig. S3, ESI†) of these photocatalysts show two characteristic peaks with the centers at around $13.1°$ and $27.3°$, which result from the inter-plane and intra-plane periodic stacking units in g-C_3N_4, respectively. The unchanged XRD patterns after the reactions suggest a good retention of the crystal structure of g-C_3N_4.

The chemical states of carbon and nitrogen of g-C_3N_4 photocatalysts were investigated using X-ray photoelectron spectroscopy (XPS). Fig. 3 compares the XPS spectra of C 1s and N 1s in bulk g-C_3N_4 before and after the reaction. Two major peaks of C 1s at 284.6 and 288.2 eV originate from adventitious carbon and C–$(N)_3$ (the main state of C in g-C_3N_4), respectively.[23] In the spectra of N 1s, two peaks at 398.6 and 400.3 eV are assigned to the nitrogen species in the forms of N–$(C)_2$ and N–$(C)_3$, respectively.[23] The spectra of O 1s show oxygen species adsorbed on g-C_3N_4 with a binding energy of inner core electrons at 532 eV. No binding energy shift or new peak after the reaction is detected in the C 1s, N 1s and O 1s spectra. The analysis of the chemical states of C, N and O of the nanosheets
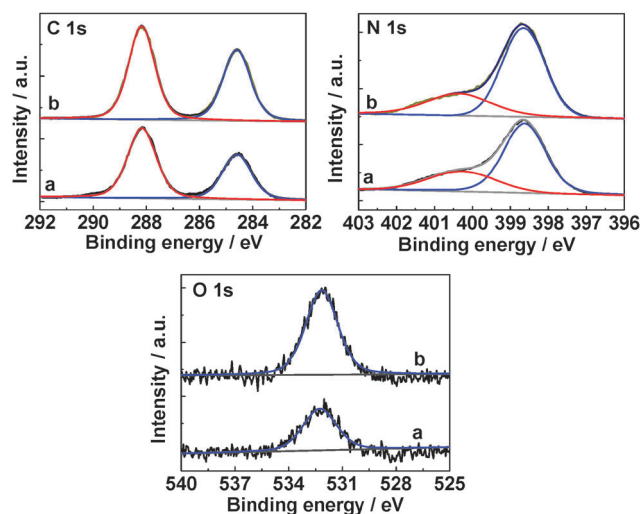
Fig. 3 Comparison of high resolution XPS spectra of C 1s, N 1s and O 1s of bulk g-C_3N_4 (a) before and (b) after CO_2 photoreduction under UV-visible light.

also supports no binding energy shift and the absence of a new peak (Fig. S4, ESI†). Overall, the chemical states of lattice carbon and nitrogen in g-C$_3$N$_4$ samples remain unchanged after the reactions. These results together with the analysis from SEM and XRD suggest a good stability of g-C$_3$N$_4$ photocatalysts in CO$_2$ photoreduction.

According to the literature, three different mechanisms for the conversion of CO$_2$ into methane on the semiconductor surface have been proposed. These involve the production of three different intermediates: formaldehyde, carbene and glyoxal.[2] Considering the presence of CH$_3$CHO in the final products, the mechanism of photoreduction of CO$_2$ on g-C$_3$N$_4$ photocatalysts could follow the glyoxal pathway containing the dimerization process (Fig. S5, ESI†).[2] Since the completion of the glyoxal pathway involves both the reduction and oxidation processes, efficient transfer of photo-generated electrons and holes from g-C$_3$N$_4$ to the reactants are essentially important for the production of CH$_4$ as the product at the end of this pathway. Based on the result that the major final product with bulk g-C$_3$N$_4$ is CH$_3$CHO while the major final product with the nanosheets is CH$_4$, it is reasonably inferred that the oxidation of CH$_3$CHO and subsequent reduction process on bulk g-C$_3$N$_4$ is limited. This inference is further supported by the fact that bulk g-C$_3$N$_4$ produces a much lower amount of the CO byproduct in the photoreduction of CO$_2$ than g-C$_3$N$_4$ nanosheets.

Band structure is a crucial factor affecting CO$_2$ photoreduction. The pioneering work on the photoelectrocatalytic reduction of CO$_2$ in aqueous solution by Inoue et al. showed a positive dependence of the reactivity of CO$_2$ reduction on the energy level difference between the conduction band of the semiconductor and the redox agents in the solution by comparing a group of semiconductors with different conduction band minima.[1] This was explained by saying that a large energy level difference increases charge carrier transfer rate between the photogenerated carriers and the solution species. Recent progress[24–26] has shown that wide-bandgap semiconductors with a high conduction band level (more negative) give a high reactivity of CO$_2$ photoreduction, which supports this hypothesis. In our case, compared to bulk g-C$_3$N$_4$, the nanosheets have a larger bandgap by 0.2 eV as a result of a lower valence band edge by 80 meV (Fig. S6, ESI†) and high conduction band edge by 120 meV, as illustrated in Fig. 4. This means that, compared to bulk g-C$_3$N$_4$, the nanosheets can provide a stronger driving force for the transfer of holes or electrons as a result of the larger energy level difference between the electronic band edges and the redox potentials of the reactants (Fig. 4). In this situation, fast photoexcited electron transfer to the intermediate species in all elementary steps of producing CH$_4$ is favorable and feasible. In contrast, the relatively slow electron transfer rate of bulk g-C$_3$N$_4$ greatly lowers the probability of the latter elementary steps occurring. In addition, in contrast to the bulk, the nanosheets can generate a larger percentage of long-lived charge carriers under the light irradiation.[22] This increases the probability of photo-generated electrons and holes in involving the reduction of CO$_2$ to CH$_4$ production.

The high specific surface area of the nanosheets may have an impact on the photoreduction of CO$_2$. There is no doubt that if all the other parameters of the photocatalysts are comparable, the
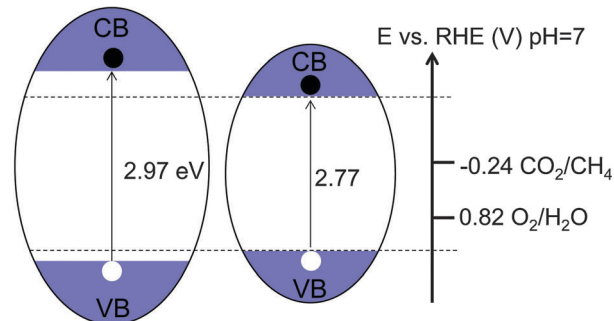
Fig. 4 Schematic of the band structures of bulk g-C$_3$N$_4$ (the right panel) and g-C$_3$N$_4$ nanosheets (the left panel) referred to the redox potentials of different redox reactions. VB: valence band; CB: conduction band.

large specific surface area of the nanosheets (306 vs. 50 m^2 g^{-1} of bulk g-C$_3$N$_4$) is favorable for photocatalytic reaction activity by providing abundant active sites for the adsorption of reactant species. This might partially favor the reduction of CO$_2$ to CH$_4$ by increasing the adsorption capability of intermediate products and thus promoting the subsequent elementary steps.

Finally, we should discuss the influence of the layer structure of g-C$_3$N$_4$ on the selectivity of CO$_2$ photoreduction. The layers in g-C$_3$N$_4$ consist of hydrogen-bonded strands of polymeric melon units as shown in Fig. 1.[27] Independent of the thickness along the c-axis of the bulk g-C$_3$N$_4$ and nanosheets studied, the surface atomic structure of the two photocatalysts can be considered to be the same. The adsorption of the reactant species is dependent on the surface atomic structure of the solid so that the adsorption state of the reactant species on g-C$_3$N$_4$ is also the same. In this situation, the photoreduction of CO$_2$ on g-C$_3$N$_4$ could follow a single reaction pathway and then stop at different elementary steps largely depending on the photoexcited carrier transfer rate as analyzed above. This may explain why only one major product was produced using g-C$_3$N$_4$ with a layered structure.

In summary, the photoreduction reactions of CO$_2$ on two g-C$_3$N$_4$ photocatalysts with different bandgaps were investigated. The dependence of the nature of the major product on the band structure of g-C$_3$N$_4$ was shown. Bulk g-C$_3$N$_4$ with a bandgap of 2.77 eV gives the major product of CH$_3$CHO and the nanosheets with a bandgap of 2.97 eV give the major product of CH$_4$. These results could provide insight into the design of efficient photocatalysts with high selectivity for CO$_2$ photoreduction conversion.

Notes and references

1 T. Inoue, A. Fujishima, S. Konishi and K. Honda, *Nature*, 1979, **277**, 637.
2 S. N. Habisreutinger, L. S. Mende and J. K. Stolarczyk, *Angew. Chem., Int. Ed.*, 2013, **52**, 7372.
3 V. P. Indrakanti, J. D. Kubicki and H. H. Schobert, *Energy Environ. Sci.*, 2009, **2**, 745.
4 S. W. Liu, J. G. Yu and M. Jaroniec, *J. Am. Chem. Soc.*, 2010, **132**, 11914.

5 G. Liu, J. Pan, L. C. Yin, J. T. S. Irvine, F. Li, J. Tan, P. Wormald and H. M. Cheng, *Adv. Funct. Mater.*, 2012, **22**, 3233.
6 X. C. Wang, K. Maeda, A. Thomas, K. Takanabe, G. Xin, J. M. Carlsson, K. Domen and M. Antonietti, *Nat. Mater.*, 2009, **8**, 76.
7 J. S. Zhang, J. H. Sun, K. Maeda, K. Domen, P. Liu, M. Antonietti, X. Z. Fu and X. C. Wang, *Energy Environ. Sci.*, 2011, **4**, 675.
8 G. Liu, P. Niu, C. H. Sun, S. C. Smith, Z. G. Chen, G. Q. Lu and H. M. Cheng, *J. Am. Chem. Soc.*, 2010, **132**, 11642.
9 Q. J. Xiang, J. G. Yu and M. Jaroniec, *J. Phys. Chem. C*, 2011, **115**, 7355.
10 L. Ge and C. C. Han, *Appl. Catal., B*, 2012, **117**, 268.
11 X. C. Wang, X. F. Chen, A. Thomas, X. Z. Fu and M. Antonietti, *Adv. Mater.*, 2009, **21**, 1609.
12 J. G. Yu, S. H. Wang, J. X. Low and W. Xiao, *Phys. Chem. Chem. Phys.*, 2013, **15**, 16883.
13 L. Ge, C. C. Han and J. Liu, *J. Mater. Chem.*, 2012, **22**, 11843.
14 X. F. Chen, J. S. Zhang, X. Z. Fu, M. Antonietti and X. C. Wang, *J. Am. Chem. Soc.*, 2009, **131**, 11658.
15 Y. J. Zhang, T. Mori, L. Niu and J. H. Ye, *Energy Environ. Sci.*, 2011, **4**, 4517.
16 G. H. Dong and L. Z. Zhang, *J. Mater. Chem.*, 2012, **22**, 1160.
17 J. Mao, T. Y. Peng, X. H. Zhang, K. Li, L. Q. Ye and L. Zan, *Catal. Sci. Technol.*, 2013, **3**, 1253.
18 Y. P. Yuan, S. W. Cao, Y. S. Liao, L. S. Yin and C. Xue, *Appl. Catal., B*, 2013, **140–141**, 164.
19 Z. J. Huang, F. B. Li, B. F. Chen, T. Lu, Y. Yuan and G. Q. Yuan, *Appl. Catal., B*, 2013, **136–137**, 269.
20 S. W. Cao, X. F. Liu, Y. P. Yuan, Z. Y. Zhang, Y. S. Liao, J. Fang, S. C. J. Loo, T. C. Sum and C. Xue, *Appl. Catal., B*, 2014, **147**, 940.
21 K. Maeda, K. Sekizawa and O. Ishitani, *Chem. Commun.*, 2013, **49**, 10127.
22 P. Niu, L. L. Zhang, G. Liu and H. M. Cheng, *Adv. Funct. Mater.*, 2012, **22**, 4763.
23 A. Thomas, A. Fischer, F. Goettmann, M. Antonietti, J. O. Muller, R. Schlögl and J. M. Carlsson, *J. Mater. Chem.*, 2008, **18**, 4893.
24 S. C. Yan, S. X. Ouyang, J. Gao, M. Yang, J. Y. Feng, X. X. Fan, L. J. Wan, Z. S. Li, J. H. Ye, Y. Zhou and Z. G. Zou, *Angew. Chem., Int. Ed.*, 2010, **49**, 6400.
25 Q. Liu, Y. Zhou, J. H. Kou, X. Y. Chen, Z. P. Tian, J. Gao, S. C. Yan and Z. G. Zou, *J. Am. Chem. Soc.*, 2010, **132**, 14385.
26 G. C. Xi, S. X. Ouyang and J. H. Ye, *Chem. – Eur. J.*, 2011, **17**, 9057.
27 B. V. Lotsch, M. Doblinger, J. Sehnert, L. Seyfarth, J. Senker, O. Oeckler and W. Schnick, *Chem. – Eur. J.*, 2007, **13**, 4969.